Fluid Dynamics &
Materials Processing

Tech Science Press

http://doi.org/10.32604/fdmp.2026.084484

ARTICLE

Mechanisms and Controlling Factors of Displacement-Front Evolution during Chemical Flooding in High Water-Cut Reservoirs

Dejun Wu[1,2,*], Chunlei Yu[1], Xuan Lu[1], Deshuo Tao[1], Xiaoning Li[1] and Hao Song[3]

[1]Exploration and Production Research Institute, Sinopec Shengli Oilfield Company, Dongying, China
[2]Postdoctoral Research WorkStation, Sinopec Shengli Oilfield Company, Dongying, China
[3]Schoold of Civil Engineering, Qingdao University of Technology, Qingdao, China
*Corresponding Author: Dejun Wu. Email: wudejun.slyt@sinopec.com

Received: 26 April 2026; Accepted: 15 June 2026; Published: 30 June 2026

ABSTRACT: To address the short peak-production period and limited incremental recovery commonly encountered during chemical flooding of high water-cut reservoirs, this study investigates the dynamic evolution of displacement fronts and their controlling factors through laboratory experiments and numerical simulation. Two-dimensional plate flooding experiments were first conducted to characterize the evolution of the oil bank in homogeneous and heterogeneous reservoirs, revealing a four-stage process of formation, enrichment, mobilization, and residual depletion. Based on water-cut behavior, the flooding process was further classified into early-response, peak-response, and late-response stages. A three-dimensional heterogeneous reservoir model was subsequently developed to quantify the spatiotemporal evolution of the pressure, oil-bank, and chemical-agent fronts. The results show a clear displacement-front sequence, with the pressure front leading, the oil bank occupying the intermediate zone, and the chemical-agent front trailing behind. Sensitivity analyses demonstrate that the flooding system, chemical concentration, and slug size significantly influence oil-bank development. Compared with polymer flooding and polymer-surfactant flooding, the heterogeneous flooding system increases the maximum oil-bank magnitude by 72% and 43%, respectively. Higher chemical concentrations promote oil-bank enrichment, although the incremental benefit gradually diminishes. In addition, a critical slug size of approximately 0.4 PV is identified, beyond which further increases yield limited improvement.

KEYWORDS: Chemical flooding; front characterization; oil bank migration; evolution patterns; physical simulation; numerical simulation; influencing factors

1 Introduction

As the primary technology for oilfield development, water flooding has been utilized for long-term exploitation, leading the vast majority of oilfields into high or even ultra-high water-cut stages, with the comprehensive water cut generally exceeding 90% [1]. At this stage, the subsurface oil–water relationship becomes increasingly complex, and the remaining oil shows a highly dispersed distribution, mainly existing as discontinuous isolated-island- and cluster-like accumulations at the pore scale or remaining trapped in low-permeability zones [2–4]. At the pore scale, long-term water flooding progressively breaks the main oil cluster into numerous isolated droplets whose size and connectivity diminish continuously with injected pore volume [5]. As a result, the oil-displacement efficiency of conventional water flooding declines sharply, and further enhancement of oil recovery faces great challenges [6]. To address the problems

of highly dispersed and difficult-to-produce remaining oil in mature and ultra-high-water-cut reservoirs, oilfields worldwide have continuously explored various enhanced oil recovery (EOR) technologies, including chemical flooding, low-salinity water flooding, gas injection, and thermal methods. Among these approaches, chemical flooding has been extensively applied and further developed in China because of the large number of mature waterflooded reservoirs that have entered the ultra-high-water-cut stage. To economically and effectively mobilize the large amount of accumulated remaining oil after the high-water-cut stage, chemical flooding technologies, including polymer flooding, surfactant flooding, heterogeneous composite flooding, and their combinations, are regarded as among the most promising tertiary oil recovery methods [7,8]. Their core mechanism is to improve the mobility ratio, enlarge the swept volume, and enhance oil-washing efficiency through chemical injection [9], thereby re-accumulating and re-grouping dispersed remaining oil to form a continuous high-saturation "oil bank", which is eventually driven to production wells [10]. Therefore, the effective formation and orderly advance of displacement fronts are key indicators of the success of chemical flooding.

Recent studies have further deepened the understanding of chemical enhanced oil recovery (CEOR) mechanisms. For instance, Liu et al. highlighted that surfactant retention and adsorption significantly influence the effective propagation of the chemical front and ultimately control the displacement efficiency [11]. Lv et al. demonstrated that advanced chemical flooding systems can improve sweep efficiency and stabilize displacement fronts in heterogeneous reservoirs [12]. Furthermore, Nagy et al. summarized that the effectiveness of CEOR is strongly governed by the dynamic evolution of displacement fronts and their interaction with reservoir heterogeneity [13]. These findings indicate that the formation, stability, and propagation of displacement fronts are essential to the success of chemical flooding processes. However, conventional chemical-flooding implementation schemes usually suffer from a "static" design deficiency. That is, once the injection pattern, chemical system, and injection parameters are determined during the design stage, the subsequent injection process lacks real-time adjustment based on subsurface dynamic response. This fixed mode is difficult to adapt to the dynamic evolution characteristics of strongly heterogeneous reservoirs in high-water-cut oilfields, often resulting in premature breakthrough of chemicals along high-permeability channels and causing fingering or tonguing of displacement fronts [14], thereby failing to effectively sweep the remaining oil in low-permeability zones [15]. The direct consequence is a short peak response period, rapid water breakthrough of the oil bank, and ultimately an incremental recovery far lower than expected. In recent years, field practice has shown that the distribution of remaining oil during chemical flooding exhibits a dynamic evolution law of "dispersion–accumulation–re-dispersion", and the oil bank undergoes a complete life cycle from formation to accumulation and mobilization [16]. During field implementation in the Gudao East area of Shengli Oilfield, staged control measures—including optimization of injection-production conditions during the initial response stage, local infill drilling during the trough-platform stage, and sidetracking to avoid water during the platform-extension stage—extended the low-water-cut trough period to 8 years and increased recovery to over 60% [17]. At the same time, extensive field practice has demonstrated that coordinated regulation of chemical dosage and well pattern can further enhance the balanced advance of displacement fronts and improve the development performance of mature high-water-cut oilfields [18]. This practice indicates that achieving a transition from "static injection" to "dynamic regulation" in chemical flooding, through accurate prediction and proactive intervention of displacement-front evolution, is an effective way to maximize chemical-flooding efficiency and improve recovery factor.

At present, extensive studies have been carried out on the mechanisms and applications of chemical flooding. Experimentally, CT scanning, nuclear magnetic resonance, microfluidics, and other techniques have been applied to laboratory physical models to realize visual observation of the displacement process [19,20].

In terms of numerical simulation, commercial software can perform detailed simulations of multiphase, multicomponent flow and analyze parameter sensitivity [21]. However, existing studies still have obvious shortcomings: (1) most studies focus on the ultimate recovery performance of chemical flooding, while lacking systematic and continuous observation and characterization of the dynamic evolution of displacement fronts over the whole life cycle [6]; (2) existing studies often analyze the influence of a single factor in isolation, without systematically considering the main controlling factors affecting front migration and their evolution laws at different stages (initial response, peak response, and late response) [22]. Therefore, this paper takes the migration laws of displacement fronts (oil bank, chemical agent, and pressure) at different response stages of chemical flooding as the main line and systematically conducts an analysis of influencing factors. First, through laboratory physical simulation experiments, the distribution characteristics and dynamic evolution laws of displacement fronts throughout the whole chemical-flooding process are monitored and characterized. Then, a representative numerical mechanism model for a typical line-drive well pattern is established to quantitatively analyze the migration laws of displacement fronts at different response stages. Finally, an influencing-factor analysis is carried out to identify the main controlling factors governing front advance at each stage and their impact laws. The primary contribution of this study mainly lies in the establishment of a stage-based displacement-front evolution framework for chemical flooding in high-water-cut reservoirs. The coupled dynamic evolution of the pressure front, chemical agent front and the oil-bank front throughout the entire chemical-flooding life cycle was systematically investigated and the controlling effects on oil-bank evolution are quantitatively analyzed, thereby providing a mechanistic basis for stage-based dynamic regulation and optimization of chemical flooding in mature heterogeneous reservoirs.

2 Experimental Section

2.1 Materials and Apparatus

2.1.1 Preparation of Plate Models

According to the actual reservoir permeability, a two-dimensional homogeneous plate model was prepared. The model dimensions were 20 cm × 20 cm × 0.5 cm, and the permeability of the homogeneous model was 1000 × millidarcy (mD), filled with 180-mesh sand mixed with 5% adhesive. The preparation procedure included bonding acrylic plates, preparing the sand mixture, filling the model, standing for 24 h, sealing, drilling, and tubing insertion. Following the same procedure, a two-dimensional heterogeneous plate model of the same size with three equal-width layers of high, medium, and low permeability was also prepared. The adhesive-sand mixtures and proportions used were 40-mesh sand with 8% adhesive, 60-mesh sand with 8% adhesive, and 80-mesh sand with 8% adhesive, respectively. Schematics of the homogeneous and heterogeneous two-dimensional plate models are shown in Fig. 1a,b, respectively.

2.1.2 Preparation of Experimental Fluids

The fluids used in the experiments mainly included formation water, simulated oil, and chemical agent. Their preparation procedures and parameters are as follows.

(1) Formation water: deionized water was used to dissolve salts, and the total salinity was 20.0749 g/L. The detailed composition was as follows: sodium chloride 17.5073 g/mL, sodium bicarbonate 0.7532 g/mL, calcium chloride 1.2238 g/mL, magnesium chloride hexahydrate 1.1334 g/mL, and potassium chloride 0.0602 g/mL.

(2) Simulated oil: white mineral oil with a viscosity of 40 mPa·s at 25°C, dyed with an appropriate amount of Sudan IV.

(3) Chemical agent: polymer 1600 mg/L, viscoelastic particles 800 mg/L, and surfactant 0.3%. The final prepared chemical system had a viscosity of 94.7 mPa·s, an interfacial tension of 4.1×10^{-3} mN/m, an elastic modulus of 12 Pa, and a particle size of 100–300 μm.

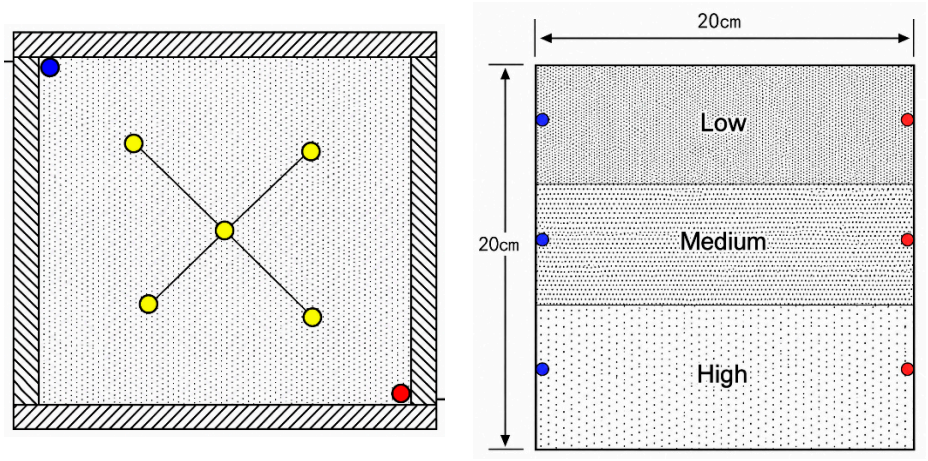

(**a**) Schematic of homogeneous model (**b**) Schematic of heterogeneous model

Figure 1: Schematic diagrams of the two-dimensional plate models: (**a**) homogeneous model; (**b**) heterogeneous model with high-, medium-, and low-permeability layers. The yellow points represent the pressure monitoring points while the blue and red points represent injection and production wells, respectively.

2.1.3 Displacement System and Displacement-Front Monitoring System

The experimental setup consisted of working fluids, constant-rate pumps, valves, piston intermediate containers, six-way valves, high-precision pressure gauges, an image and pressure acquisition system, plate models, oil–water separators, graduated cylinders, and several pipelines. Fig. 2 shows the chemical-agent displacement flow chart for the homogeneous and heterogeneous models.

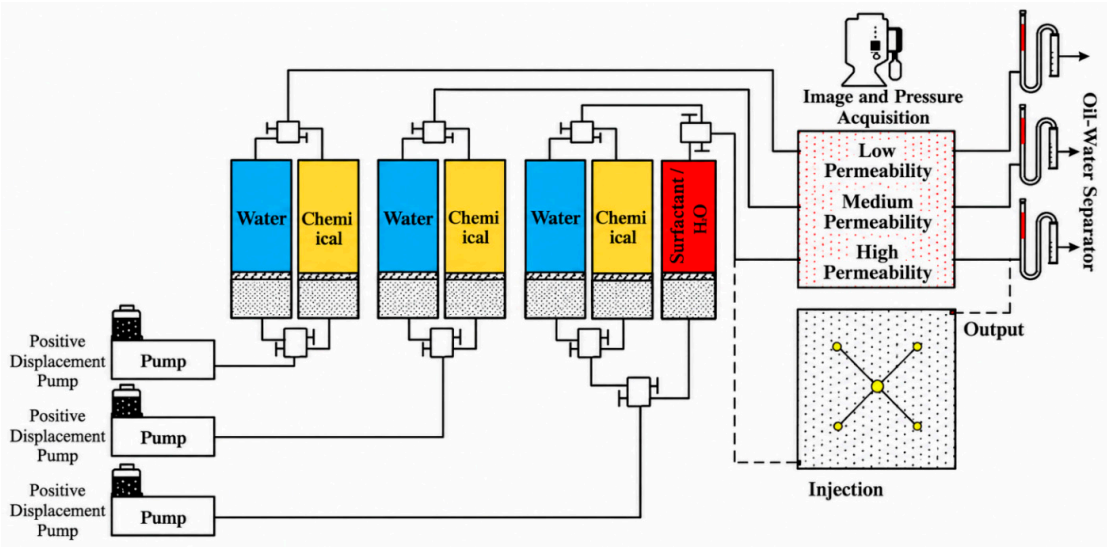

Figure 2: Schematic flow chart of chemical flooding.

2.2 Experimental Scheme and Procedure

The prepared formation water, chemical agent, and simulated oil were loaded into piston intermediate containers, and the pipelines were connected according to the flow chart shown in Fig. 2. The experimental procedure was as follows:

(1) Oil saturation of the model. The constant-rate pump was started to saturate the prepared two-dimensional plate model with simulated oil at an injection rate of 2 mL/min, and the total saturated oil volume was recorded.

(2) Water flooding. For the homogeneous model, water was injected at a constant rate (2 mL/min) to displace oil. The pressure acquisition system and oil–water separator recorded the changes in injection-end pressure, pressure at each measurement point, cumulative oil production, and cumulative liquid production with injection time. For the heterogeneous model, three pumps simultaneously injected water at a constant rate (1 mL/min) into the high-, medium-, and low-permeability layers. Oil–water separators connected to the outlets of the three layers recorded cumulative oil production and cumulative liquid production versus injection time at different times. The entire water-flooding process was recorded by the imaging equipment and transmitted to the video acquisition terminal.

(3) Chemical flooding. When the water cut at the model outlet reached 90%, chemical flooding was initiated. The camera recorded the diffusion of the chemical-agent front and oil-bank front as well as the migration of the oil bank. The pressure acquisition system recorded the injection-end pressure and the pressure at each measurement point at different times. Meanwhile, the produced fluid was separated by the oil–water separator, and the cumulative oil production and cumulative liquid production in the graduated cylinder were recorded.

(4) Data processing. The collected pressure data, images, and produced-fluid volumes were processed to study the diffusion of the chemical-agent front and oil-bank front and the migration behavior of the oil bank in the two-dimensional plate models.

2.3 Results and Discussions

2.3.1 Dynamic Variation Characteristics of Displacement Fronts during the Whole Chemical-Flooding Process in the Homogeneous Model

Fig. 3 shows the whole chemical-agent displacement process in the two-dimensional homogeneous plate model. In the figure, the white dashed line represents the chemical-agent front, and the green dashed line represents the oil-bank front. After the outlet water cut reached 90%, the injected fluid was switched to the heterogeneous system, and the advance of the chemical-agent front and oil front could be clearly observed in the model. The variation law of the oil bank obtained from the oil-saturation distributions at different times can be summarized as formation–accumulation–mobilization–residual. At the beginning of injection, a chemical-agent front formed near the injection end, and the remaining oil at the front accumulated, corresponding to the oil-bank formation stage. At approximately 0.2–0.6 PV, as the injected volume increased, the chemical-agent front continued to advance, while its advancement rate gradually slowed down. The remaining oil at the front of the agent continuously accumulated; the oil bank advanced while continuously increasing in size, and the outer edge of the oil bank moved increasingly faster, corresponding to the oil-bank accumulation stage. At approximately 0.7 PV, the outer edge of the oil bank reached the production end, and the oil bank began to be mobilized. The chemical-agent front continued to advance, corresponding to the oil-bank mobilization stage. With the continued injection of chemical agent, the accumulated oil bank was gradually produced completely, leaving residual oil.

Fig. 4 presents the relationship curves of pressure, liquid production, water production, and water cut versus injected PV during water flooding and chemical flooding in the homogeneous model. According to the variation in outlet water cut after chemical injection, the whole process can be divided into three stages: the initial response stage, the peak response stage, and the late response stage. The production characteristics of these three stages are as follows:

Initial response stage: the inlet pressure rises rapidly and quickly propagates to the outlet (0.3 PV); the chemical-agent front and oil front are formed; the outlet water cut starts to decline, and oil production begins to increase.

Peak response stage: pressure continues to rise and gradually levels off; the oil-bank front migrates while the oil-bank size keeps increasing; the water cut drops to a trough and then rebounds to about 50%, while oil production increases substantially.

Late response stage: pressure decreases slightly and then gradually stabilizes; the outer edge of the oil bank moves to the outlet; the water cut continues to increase, and oil production rises slowly and gradually becomes stable.

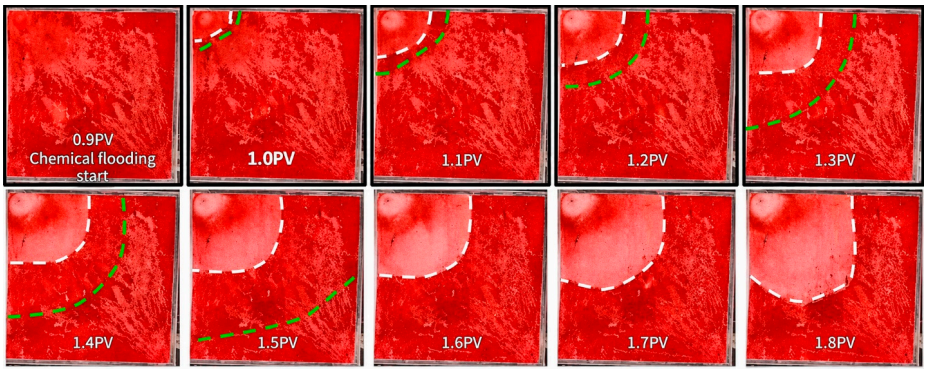

Figure 3: Whole chemical-flooding process in the homogeneous model.

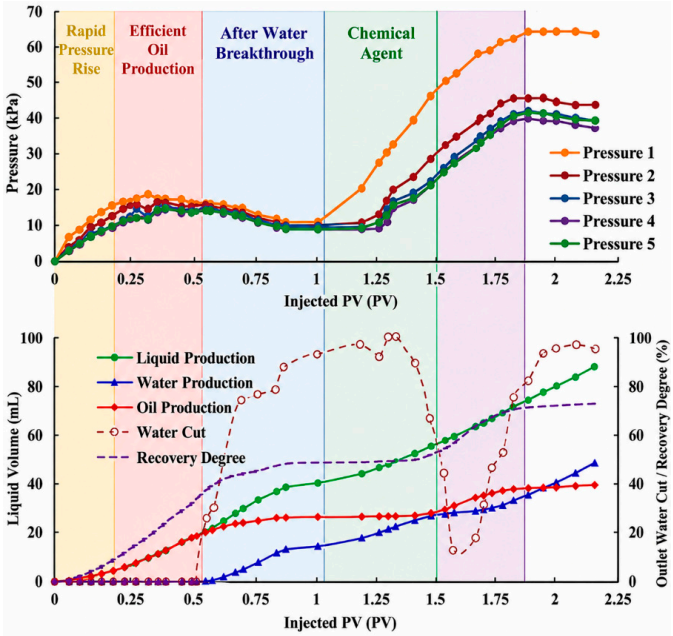

Figure 4: Relationship curves of pressure and liquid production during chemical flooding in the homogeneous model.

2.3.2 Dynamic Variation Characteristics of Displacement Fronts during the Whole Chemical-Flooding Process in the Heterogeneous Model

Fig. 5 shows the oil distribution in the heterogeneous model at different times during chemical flooding. Similarly as before, the white dashed line represents the chemical-agent front, and the green dashed line represents the oil-bank front. The oil bank as a whole still exhibits the dynamic variation law of formation–accumulation–coalescence–mobilization–residual. During injection of 0–0.4 PV, the oil bank preferentially formed in the high-permeability layer. During injection of 0.4–1.8 PV, the oil banks in the medium- and low-permeability layers formed successively with continued chemical injection; in the high- and medium-permeability layers, the oil and chemical fronts advanced obviously, and the oil-bank size gradually increased during the advancement. At about 1.0 PV, the oil fronts in the high- and medium-permeability reservoirs merged and advanced forward in a distinct step-like manner, while the oil-bank size continued to increase; afterward, the step-like oil front gradually tended to advance more uniformly. At 1.8 PV, the outer edge of the oil bank in the high-permeability layer advanced to the outlet. After 2.0 PV of chemical injection, the boundary of the high-oil-saturation zone became blurred, and the oil bank almost disappeared. The step-like advancement of the oil front is primarily caused by the different propagation velocities among layers, where the high-permeability layer responds first while the medium- and low-permeability layers lag behind because of their higher flow resistance. As chemical injection continues, the pressure field gradually redistributes between layers, weakening the interlayer displacement imbalance and promoting a more coordinated advance of the displacement fronts. Meanwhile, the enhanced mobility control effect of the chemical system suppresses preferential flow in the high-permeability layer and improves sweep in the medium- and low-permeability layers, causing the initially separated fronts to gradually coalesce into a more uniform displacement interface. This gradual coalescence suggests improved vertical sweep coordination and reduced interlayer mobility contrast during chemical flooding. Therefore, the evolution from a stepped front to a more continuous displacement interface may serve as an indicator of improved vertical conformance during chemical flooding.

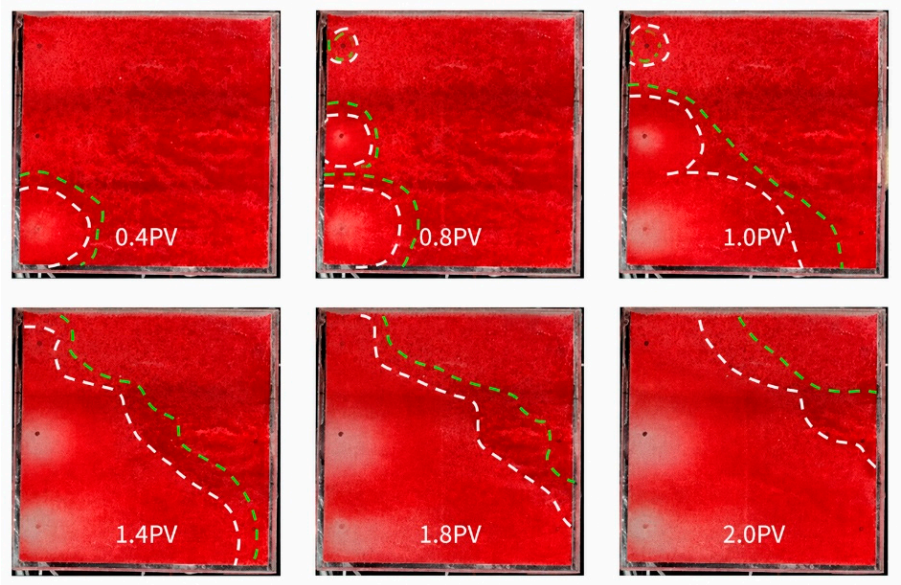

Figure 5: Oil distribution in the heterogeneous model at different times during chemical flooding.

3 Numerical Section

3.1 Establishment of the Numerical Model

To further explain the migration characteristics of displacement fronts observed in the physical simulation experiments and quantitatively analyze their influencing factors, a three-dimensional heterogeneous reservoir mechanism model (Fig. 6) was established using a commercial reservoir simulator based on the geological model of an actual block. Numerical simulation was conducted on the spatiotemporal evolution of the oil-bank, chemical-agent, and pressure fronts. The model had an average porosity of 0.31, an average permeability of 3086 mD, and a burial depth of approximately 2000 m. The grid system consisted of 25 × 27 × 3 cells, for a total of 2025 cells, with a grid spacing of about 20 m × 20 m × 3 m. The well pattern was a staggered line-drive pattern with 5 injectors and 10 producers, and the injection–production rate was 0.075 PV/a. The full process of "pre-water flooding (water cut > 95%)—0.4 PV heterogeneous composite flooding—subsequent water flooding (water cut 98%)" was simulated.

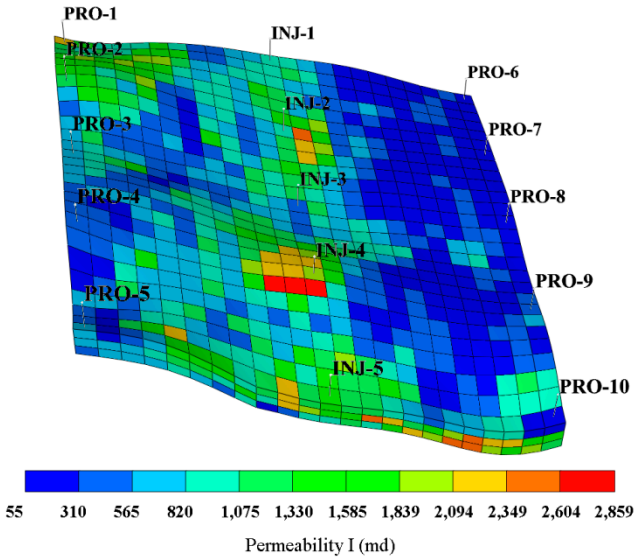

Figure 6: Schematic of the mechanism model.

The numerical model was constructed using the STARS module of CMG to describe the coupled flow and transport of oil, water, and chemical agents during heterogeneous composite flooding. The governing equations were based on components mass conservation and Darcy's law. In the model, the polymer was used only to represent the viscosity-enhancement effect of the aqueous phase, and polymer adsorption and degradation were not considered. The surfactant was mainly used to reduce the oil–water interfacial tension, and its effect was reflected by modifying the relative permeability curves. The pre-formed particle gels used in the heterogeneous composite flooding were represented by adsorption/retention and plugging effects, which reduced the effective permeability of high-permeability channels and promoted flow diversion. The fluid viscosity was updated according to the local polymer concentration, thereby reflecting the variation of aqueous-phase mobility during chemical flooding. The initial viscosity of the flooding system was different from the value used in the flooding experiments since the numerical model represents an effective *in-situ* mobility-control behavior rather than direct replication of laboratory rheology. Since the primary focus of this study is the macroscopic evolution of displacement fronts, particularly the dynamic behavior of the oil bank during chemical flooding, the numerical model mainly captures the dominant mobility-control and

oil-displacement effects of the chemical system. Detailed physicochemical transport mechanisms, including surfactant adsorption, retention, inaccessible pore volume effects, and chromatographic separation among different chemical components, were not fully resolved in the present model. These processes may broaden the chemical-agent front, reduce the effective chemical concentration, and influence the long-term stability of the oil–agent mixed zone and oil bank. Nevertheless, the current model remains suitable for analyzing the large-scale migration characteristics and stage-dependent evolution laws of displacement fronts. More rigorous coupling between multiphase flow and detailed chemical transport chemistry will be investigated in future work.

3.2 Quantitative Characterization of Displacement-Front Parameters

Based on the calculated pressure, oil saturation, and chemical concentration fields from reservoir numerical simulation, the displacement fronts were characterized to support subsequent migration-law analysis and stage comparison.

(1) In this study, the oil-bank front is defined based on the oil saturation difference between chemical flooding and the end of water flooding, as expressed in Eq. (1):

$$\Delta S_{i,j}^{o} = S_{i,j}^{ocf} - S_{i,j}^{owf} \tag{1}$$

where $S_{i,j}^{owf}$, $S_{i,j}^{ocf}$ and $\Delta S_{i,j}^{o}$ represent the oil saturation of grid cell (i, j) at the end of water flooding, during chemical flooding and the oil saturation change, respectively. Based on the results of the above laboratory displacement experiments, under the strong oil-washing action of the chemical agent, the dispersed remaining oil after water flooding is re-accumulated to form an oil bank. The saturation change value in the oil-bank region is positive. Therefore, this study proposes the following formula to define the oil-bank region:

$$\Omega_{oilwall} = \{(i, j) | \Delta S_{i,j}^{o} > 0\} \tag{2}$$

(2) The chemical agent front is characterized as follows. Based on reservoir numerical simulation, the concentration field of the chemical agent during the chemical flooding process is obtained, denoted as $C_{i,j}^{wcf}$. A threshold concentration, typically defined as 10%–30% of the maximum concentration, is employed as the criterion for identifying the chemical agent front given by Eq. (3):

$$C_{threshold} = s \cdot C^{wcf\_\max} \tag{3}$$

where s is the threshold coefficient, generally 10%–30%, and $C^{wcf\_\max}$ is the maximum value of the chemical concentration field. The selection of the threshold has an important influence on the accuracy of chemical-agent-front identification. After determining the concentration threshold, the region in which the chemical concentration satisfies the criterion is extracted by systematically examining and screening all simulation grid cells throughout the reservoir that satisfy Eq. (4):

$$C^{wcf} > C_{threshold} \tag{4}$$

This region is the spatial range in which the chemical-flooding agent exerts an effective displacement effect in the reservoir. Its geometric shape and spatial distribution can directly reflect the sweep efficiency of chemical flooding, the adaptability of the injector–producer pattern, and the influence of reservoir heterogeneity on chemical-flooding performance. By extracting the boundary contour of this region, the spatial distribution of the chemical-agent front can be obtained.

(3) The pressure front is characterized as follows. Based on reservoir numerical simulation, the pressure fields during chemical flooding and at the end of water flooding are obtained, denoted as $P_{i,j}^{cf}$ and $P_{i,j}^{wf}$, respectively. By comparing the pressure field distributions between these two stages, a pressure difference field is calculated to quantify the impact of chemical flooding on the reservoir pressure distribution:

$$\Delta P_{i,j} = P_{i,j}^{cf} - P_{i,j}^{wf} \tag{5}$$

where $\Delta P_{i,j}$ is the pressure change at a grid cell. This pressure-difference field can clearly show the distribution of formation-pressure increment caused by chemical-agent injection. A positive value indicates that the pressure at that location increases because of chemical flooding, which is usually closely related to the sweep of the chemical agent, mobility control, and changes in displacement resistance. The spatial distribution and magnitude of the pressure-increase region can directly reflect the sweep range and action intensity of the chemical agent. The region with a significant pressure increase is then extracted, where $\Delta P_{threshold}$ is the pressure-change threshold determined according to actual reservoir conditions and is generally taken as 0.3–1.0 MPa:

$$\Delta P_{i,j} > \Delta P_{threshold} \tag{6}$$

Finally, a boundary-recognition algorithm is used to extract the boundary contour of the region with a significant pressure increase, thereby obtaining the precise spatial distribution of the pressure front. We remark that, unlike the saturation or concentration fronts, the pressure front is not a unique physical interface but rather a threshold-defined pressure influence zone. The reason is that pressure propagation is governed primarily by pressure diffusion, whereas saturation and concentration evolution are controlled by convective multiphase flow and chemical transport. Therefore, although the selected pressure threshold affects the exact shape and extent of the identified pressure front, the overall migration trend and the relative positional relationship among the pressure, chemical-agent, and oil-bank fronts remain robust as is demonstrated in Fig. 7 where two pressure fronts based on two different threshold values are shown.

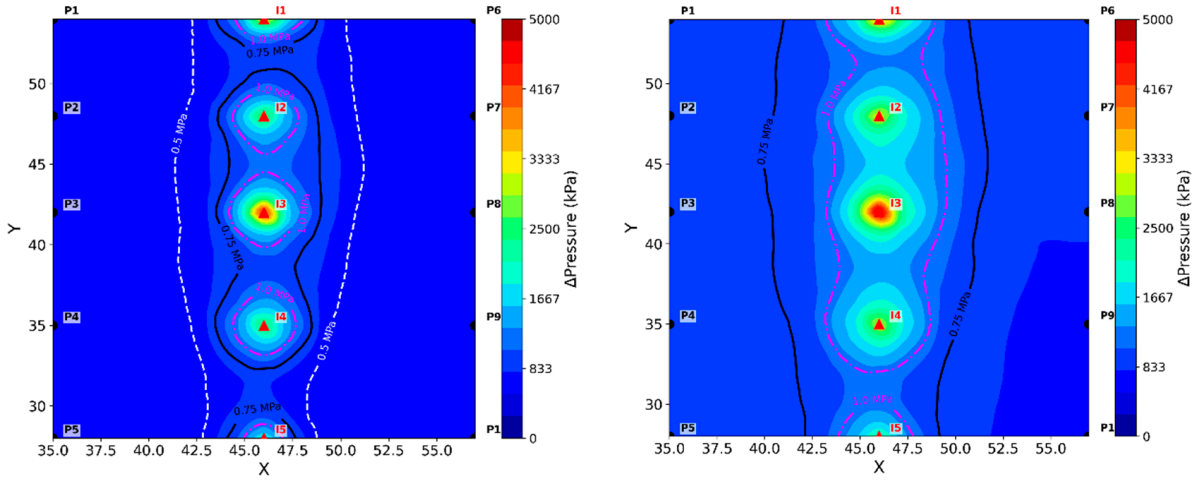

Figure 7: Effect of pressure-change threshold on the identified pressure-front position. The left panel uses a threshold of 0.5 MPa, and the right panel uses a threshold of 0.75 MPa. The white dashed and black solid lines denote the pressure-front positions at 0.08 PV and 0.16 PV injected, respectively.

3.3 Migration Laws of Displacement Fronts

The saturation values of the grid cells along the injector–producer line at the middle position of the plane in the third layer of the mechanism model were extracted, and the variation law of oil-bank saturation at different grid positions between the injector and producer was plotted, as shown in Fig. 8. It can be seen that the oil bank exhibits a prominent feature of "advancing while accumulating" during chemical flooding: the oil-bank front continuously advances toward the production well, while the oil saturation within the oil bank keeps increasing, the maximum saturation rises, and the oil-bank coverage continuously expands. When it reaches the vicinity of the production well, both the maximum saturation and the oil-bank size reach their maxima. Thereafter, as the oil bank is gradually produced, the maximum saturation continuously decreases, and some oil eventually remains. This migration feature, characterized by simultaneous advance and accumulation, fully reflects the effective oil-displacement action of the chemical agent and the dynamic accumulation mechanism of the oil bank. The numerical simulation results show that the oil bank also exhibits the feature of "advancing while accumulating" during chemical flooding, which is consistent with the "formation–accumulation–mobilization–residual" evolution process observed in the physical simulation experiments.

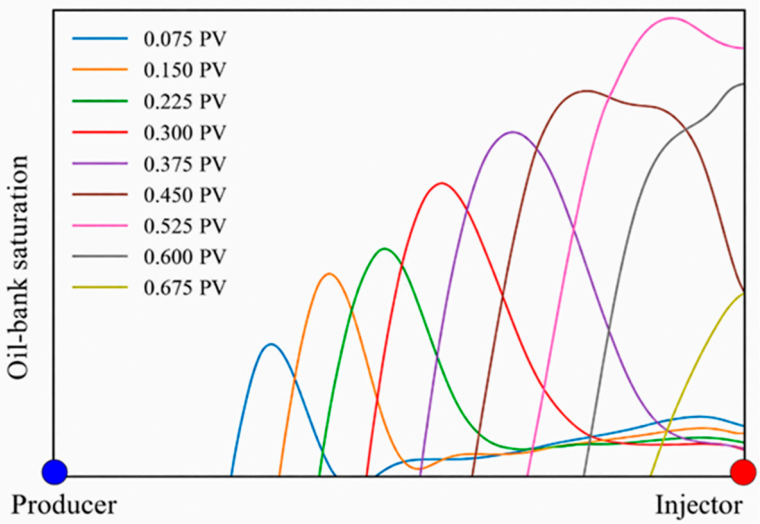

Figure 8: Oil-bank saturation at different positions between injector and producer at different time steps.

Figs. 9 and 10 show the spatial positional relationship of the three fronts along the main flow direction at the same moment. The pressure front is located at the foremost position, the oil bank is in the middle, and the chemical-agent front lags behind. This sequence indicates the seepage-flow characteristic of "pressure propagation before mass transport". The pressure front first disturbs the reservoir pressure field and provides the driving force for oil-bank migration. The oil bank forms and advances behind the pressure front due to the accumulation of mobilized oil, whereas the chemical-agent front migrates more slowly because its transport is affected by convection, dispersion, adsorption/retention, and interaction with the porous medium.

Therefore, the reservoir can be divided into three zones according to the relative positions of the fronts: the pressure-affected zone ahead of the oil bank, the oil-bank accumulation zone between the pressure front and the chemical-agent front, and the chemical-agent swept zone behind the chemical-agent front. This front-advancement sequence is consistent with the results of the two-dimensional plate-model experiments, further confirming the characteristic of "pressure propagation before mass transport". Based on the oil-bank morphology and the corresponding water-cut variation in the physical simulation experiments, the

chemical-flooding process was divided into three stages: initial response, peak response, and late response. Fig. 11 shows the typical oil-bank distributions at these stages. Future work should quantitatively calibrate relative permeability and capillary pressure functions using experimentally observed front morphology and production dynamics.

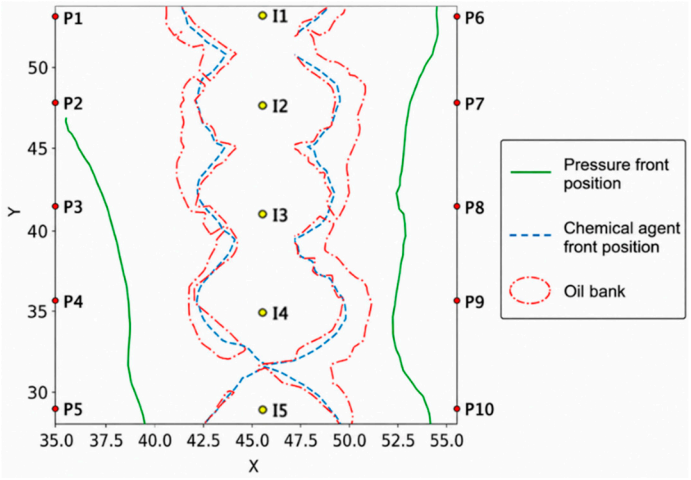

Figure 9: Schematic of the relative positional relationship of the three fronts ("oil–agent–pressure") at the same moment.

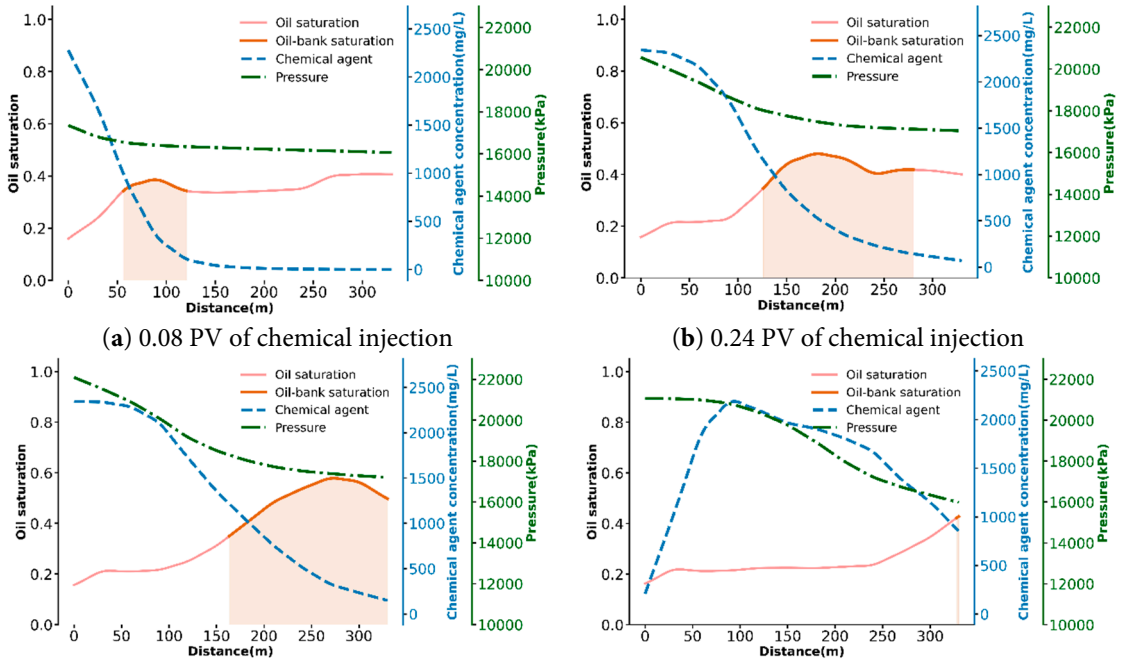

(**a**) 0.08 PV of chemical injection

(**b**) 0.24 PV of chemical injection

(**c**) 0.32 PV of chemical injection

(**d**) 0.16 PV of subsequent water flooding

Figure 10: Evolution of the relative positions of the pressure front, oil-bank front, and chemical-agent front during chemical flooding: (**a**) early stage of chemical injection (0.08 PV); (**b**) intermediate stage (0.24 PV); (**c**) advanced stage (0.32 PV); and (**d**) subsequent water-flooding stage (0.16 PV).

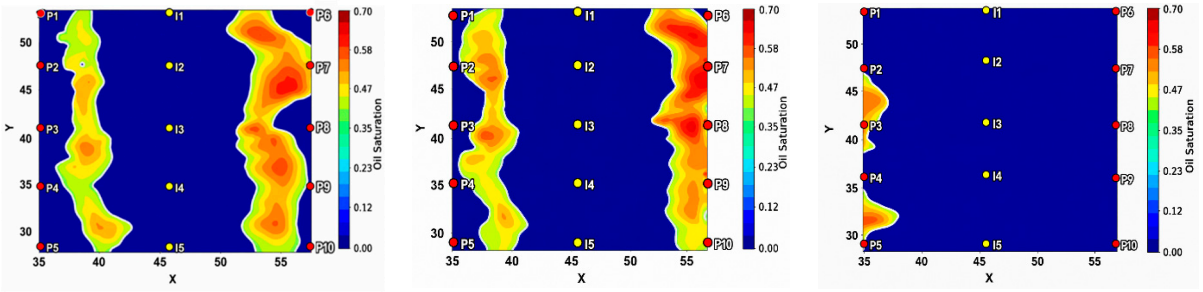

(**a**) Initial response stage (**b**) Peak response stage (**c**) Late response stage

Figure 11: Oil-bank distribution at different response stages: (**a**) initial response stage when oil bank is formed and transported to the production wells; (**b**) peak response stage when oil bank reaches the production wells; (**c**) late response stage when the oil bank is produced by the production wells.

To quantitatively characterize the size of the oil bank and its dynamic variation, a grid-cell-based calculation method for oil-bank size was established. The oil-bank size was calculated as follows:

$$J_{owall} = \left\{ \sum_{j=1}^{n} \left[\sum_{i=1}^{m} \left(S_{i,j}^{owall} \times V_{i,j}^{grid} \times \phi_{i,j} \right) \right] \right\} \rho_o / B_o \tag{7}$$

where J_{owall} is the oil-bank size, with a unit of 10^4 t; $V_{i,j}^{grid}$ is the grid-cell volume, with a unit of 10^4 m^3; $\phi_{i,j}$ is the porosity of the grid cell; and ρ_o is the crude-oil density, with a unit of t/m^3.

The oil-bank size at different time steps during chemical flooding in the mechanism model was calculated, and the variation curve of oil-bank size was plotted, as shown in Fig. 12. The evolution curve clearly shows that the oil bank undergoes four typical stages: formation, accumulation, mobilization, and residual. During the formation and accumulation stages, the oil-bank size continuously increases. After entering the mobilization stage, the oil bank starts to be produced through production wells, and its size gradually decreases. Eventually, a residual-oil distribution is formed between wells.

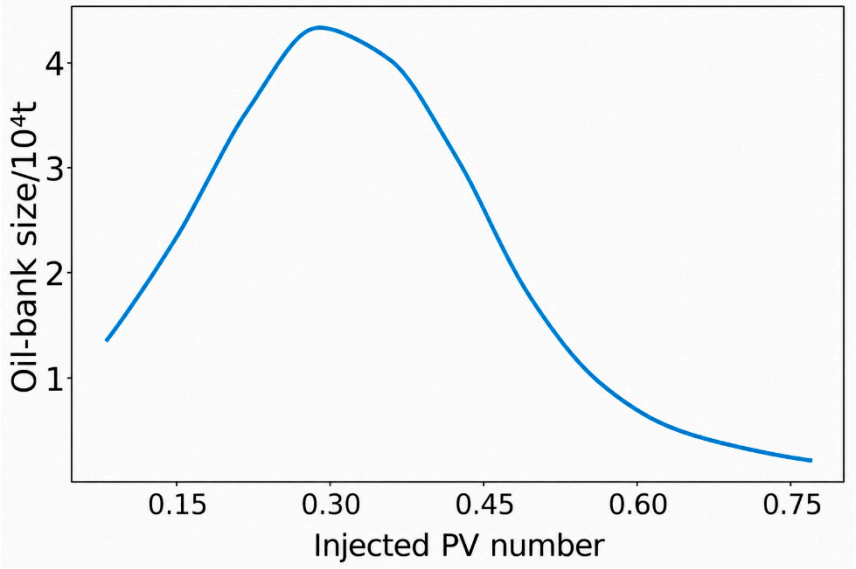

Figure 12: Variation process of oil-bank size during front migration in chemical flooding.

3.4 Study on Influencing Factors of Displacement-Front Migration

Because physical simulation experiments have certain limitations in parameter regulation and scale extension, numerical simulation was further used to carry out parameter-sensitivity analysis and systematically study the effects of flooding system, chemical concentration, injection–production rate, and slug size on displacement-front migration.

3.4.1 Effect of Different Flooding Systems

Under the premise of keeping the well pattern, injection–production rate, and injected slug size unchanged, the laws of oil-bank accumulation, migration, and mobilization under three typical chemical flooding systems—polymer flooding, binary flooding (polymer + surfactant), and heterogeneous composite flooding—were analyzed. The dynamic evolution characteristics of the oil bank in the four stages of formation, accumulation, mobilization, and residual throughout the displacement process under different chemical systems were tracked. Fig. 13 compares the oil-bank distributions under the three flooding systems at the same moment. Significant differences can be observed in oil-bank thickness, saturation, and continuity among the different systems. The oil bank formed by heterogeneous composite flooding is thicker, has higher oil saturation, and shows more uniform areal/vertical accumulation; its front also advances more stably as a whole. Binary flooding ranks second: while increasing viscosity to improve the mobility ratio, it also reduces interfacial tension, so the continuity and accumulation degree of the oil bank are significantly better than those of simple polymer flooding. Polymer flooding mainly relies on viscosity increase and has limited ability to constrain heterogeneous channels; therefore, the peak saturation and continuity of the oil bank are relatively weak. Fig. 14 shows the variation curves of oil-bank size with time under the three flooding systems, further confirming the above understanding: heterogeneous composite flooding has the largest peak oil-bank size and the longest duration of high-scale maintenance, indicating that its selective plugging of high-permeability channels can effectively suppress dominant-channel channeling, enlarge the swept volume, and promote continuous accumulation and mobilization of remaining oil in medium- and low-permeability layers. The peak value and duration of oil-bank size decrease successively for binary flooding and polymer flooding. Therefore, in strongly heterogeneous reservoirs, it is preferable to adopt a PPG system with profile-control capability, and it can be combined with binary flooding or polymer flooding to achieve the synergistic enhancement of "profile control + oil washing".

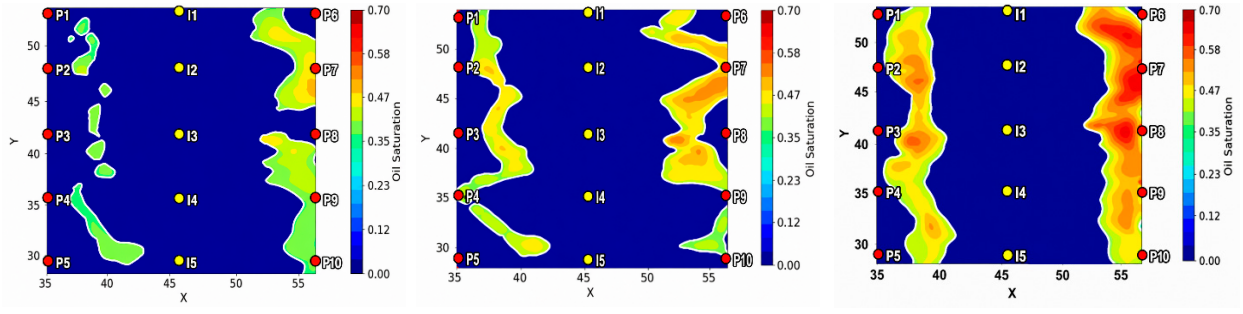

(**a**) Polymer flooding (**b**) Polymer-surfactant flooding (**c**) Heterogeneous composite flooding

Figure 13: Comparison of oil-bank distributions under different flooding systems at the same injected pore volume: (**a**) polymer flooding; (**b**) polymer–surfactant flooding; and (**c**) heterogeneous composite flooding.

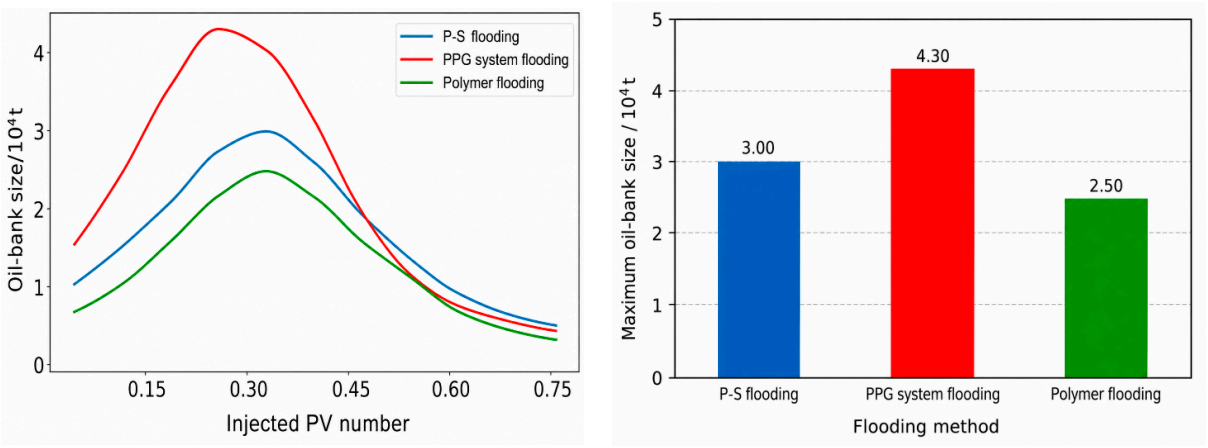

Figure 14: Variation process of oil-bank size under different flooding systems; the left plot shows the evolution of the oil-bank size as a function of injected PV number and the right plot compares the maximum oil-bank size.

3.4.2 Effect of Different Chemical Concentrations

Within the framework of heterogeneous flooding, only the mass concentration of the chemical agent (1000, 1500, 2000, and 2500 mg/L) was changed, while all other parameters remained the same as in the base case, in order to clarify the influence of concentration on oil-bank formation intensity, front-propagation velocity, and effective-period duration. Fig. 15 shows the oil-bank distributions at the same moment under different chemical concentrations. It can be seen that as the chemical concentration increases, both the peak oil-bank saturation and the width of the high-saturation zone increase overall; the oil bank gradually changes from discrete to continuous accumulation, and the front-advancement process becomes more stable. This indicates that a high-concentration system has stronger viscosity-increasing and flow-control capabilities, which can suppress channeling in dominant channels while improving the displacement intensity in medium- and low-permeability zones. Similarly, Fig. 16 compares the variation curves of oil-bank size with time under different chemical concentrations. The results show that increasing concentration significantly enlarges the oil-bank size and causes the peak to appear earlier, indicating that concentration not only affects the ultimate accumulated amount of the oil bank but also determines the kinetics of oil-bank establishment and propagation. It should be noted that the gain brought by increasing concentration is not linear: in the high-concentration range, the increases in oil-bank saturation and size tend to converge, suggesting a phenomenon of diminishing marginal benefit. Overall, chemical concentration is a key parameter controlling oil-bank accumulation intensity and flooding performance. In field applications, on the premise of meeting injectivity and anti-plugging requirements, an integrated technical–economic evaluation should be carried out by considering chemical cost and incremental oil benefit so as to determine the optimal concentration range with both significant effect and reasonable marginal benefit.

3.4.3 Effect of Different Injection Volumes

The laws of oil-bank accumulation, migration, and mobilization under four different chemical slug sizes (0.2 PV, 0.4 PV, 0.6 PV, and 0.8 PV) were comparatively analyzed to systematically reveal the influence mechanism of chemical injection volume on displacement-front migration and to provide a scientific basis for optimizing chemical-flooding injection schemes. Under different slug sizes, the oil-bank distributions at the same moment are shown in Fig. 17, and the variation curves of oil-bank size with time are shown in Fig. 18. The results show that increasing the chemical slug size can raise the peak oil-bank saturation and

enlarge the accumulated-zone range, indicating that a more sufficient supply of effective chemical agent is conducive to maintaining stronger mobility control and oil-washing effects. However, in the reservoir model investigated in this study, when the slug size exceeds about 0.4 PV, the differences among the oil-bank saturation curves gradually decrease, and the growth space of oil-bank accumulation becomes progressively smaller. This suggests that the improvement in oil-bank accumulation intensity shows a certain threshold effect under the present geological and development conditions. Under larger-slug conditions, the oil bank can still maintain a longer growth period and a slower decline stage, but the incremental benefit tends to weaken. Therefore, 0.4 PV can be regarded as a relatively effective reference slug size for the model studied in this paper. It should be noted that this value is not universal and may vary with reservoir heterogeneity, fluid properties, well pattern, and injection–production parameters. In practical applications, the optimal slug size should be further determined by combining reservoir-specific numerical simulation, economic evaluation, and field performance.

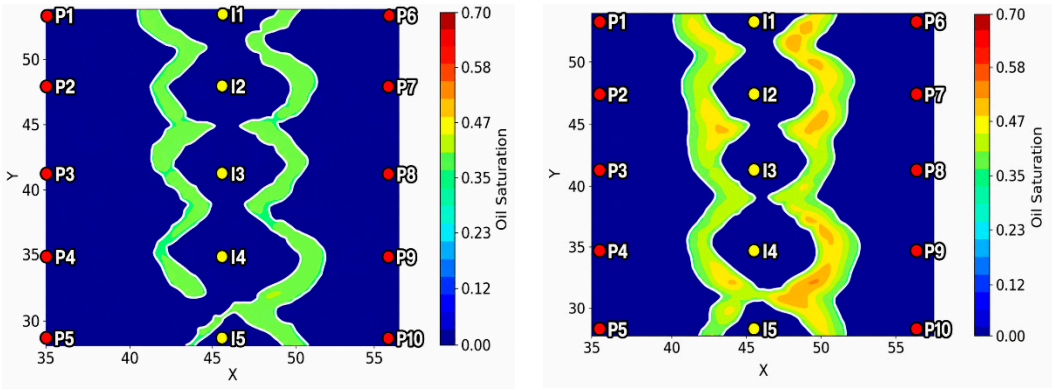

(**a**) 1500 mg/L (**b**) 2500 mg/L

Figure 15: Comparison of oil-bank distributions under different chemical concentrations at the same injected pore volume: (**a**) 1500 mg/L; (**b**) 2500 mg/L.

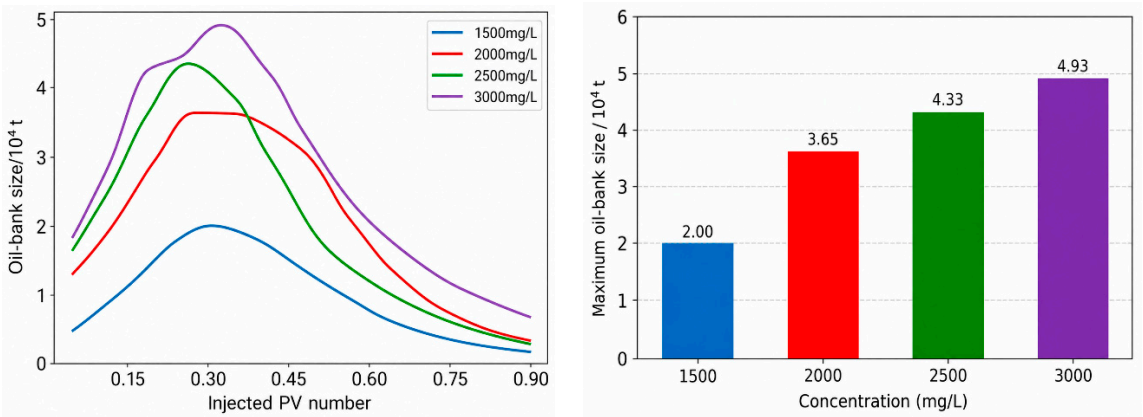

Figure 16: Variation process of oil-bank size under different chemical concentrations; the left plot shows the evolution of the oil-bank size as a function of injected PV number and the right plot compares the maximum oil-bank size.

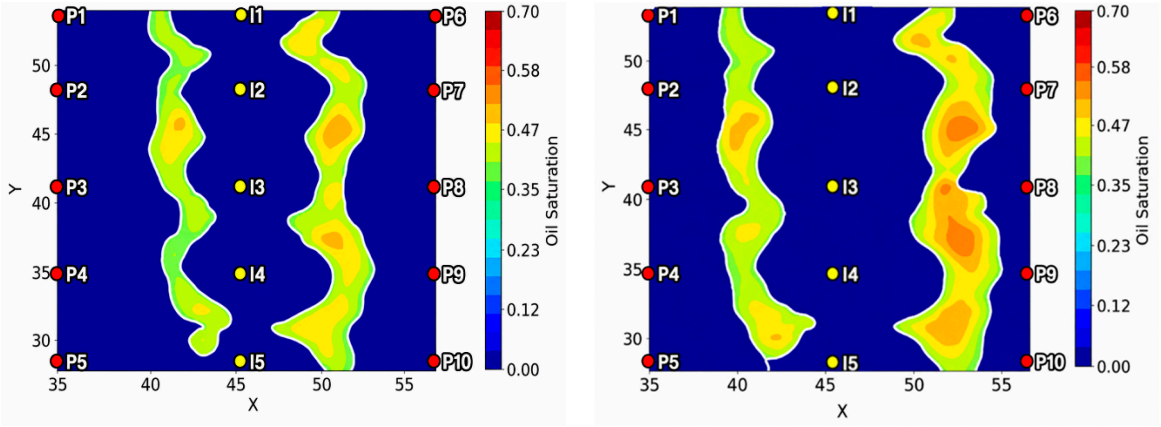

(**a**) 0.2 PV (**b**) 0.4 PV

Figure 17: Comparison of oil-bank distributions under different chemical slug sizes at the same injection stage: (**a**) 0.2 PV; (**b**) 0.4 PV.

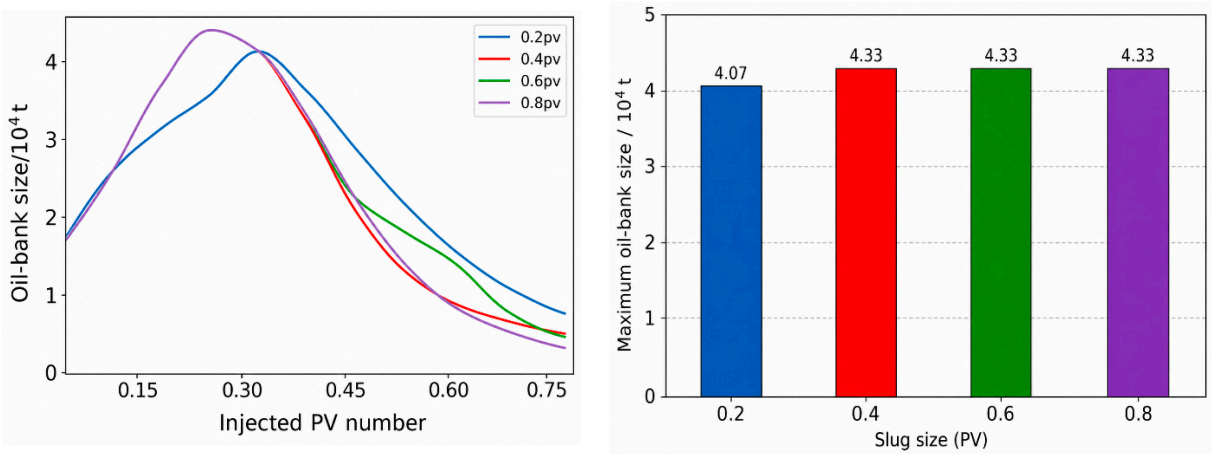

Figure 18: Variation process of oil-bank size under different total chemical volumes. The left plot shows the evolution of the oil-bank size as a function of injected PV number and the right plot compares the maximum oil-bank size.

Through the above comparative analysis, it can be concluded that chemical slug size is a key parameter affecting oil-bank accumulation intensity, displacement duration, and oil-displacement performance. Increasing the chemical slug can significantly improve oil-bank saturation, enlarge oil-bank size, reduce water cut, and prolong the effective period; however, when the injection volume exceeds 0.4 PV, the improvement effect gradually weakens. Therefore, in practical applications, the optimal slug size should be determined by comprehensively considering economic benefits.

4 Discussions and Limitations

Considering the migration laws of the pressure front, chemical-agent front, and oil-bank front, as well as the influencing-factor analysis, the implementation of chemical flooding should be regulated dynamically based on the flooding stage. During the initial response stage, the pressure front propagates rapidly while the chemical-agent front and oil bank are still forming. At this stage, priority should be given to establishing a stable and balanced pressure field through optimized injection–production allocation and profile-control measures to suppress preferential flow through high-permeability channels and promote uniform advancement

of the chemical-agent front. During the peak response stage, the oil bank undergoes rapid accumulation and mobilization, and the morphology and stability of the chemical-agent front become the key controlling factors affecting sweep efficiency. During the late response stage, the oil bank gradually approaches production wells and enters the mobilization and depletion phase. At this stage, the injection–production system should be optimized to control excessive water cycling and improve residual-oil recovery efficiency, for example through localized infill adjustment, or sidetracking in remaining-oil-enriched zones.

Although this study systematically investigated the dynamic evolution of displacement fronts during chemical flooding through integrated physical simulation and numerical simulation, several limitations should be acknowledged. First, the two-dimensional visual plate models cannot fully reproduce the complex three-dimensional interlayer crossflow, gravity segregation, and well-pattern effects present in actual reservoirs. Second, the numerical model mainly focused on macroscopic front migration behavior, while detailed physicochemical processes such as surfactant adsorption, retention, inaccessible pore volume, and chromatographic separation were simplified, which may influence the long-term evolution of the chemical-agent front and oil–agent mixed zone. Third, the laboratory chemical system viscosity was measured under surface experimental conditions, whereas shear degradation and thermal degradation under deep reservoir conditions may reduce the effective *in-situ* viscosity and alter mobility-control behavior. In addition, the characterization of the chemical-agent front and pressure front depends on selected threshold parameters, which may affect the exact front boundaries although the overall migration trends remain consistent. Finally, the quantitative conclusions obtained in this study, including the approximate 0.4 PV threshold effect of slug size, are influenced by the specific reservoir heterogeneity, mobility ratio, and well-pattern configuration adopted in the model, and therefore should not be directly regarded as universally applicable values. Future work should further incorporate field-history matching, more detailed chemical transport mechanisms, and fully coupled three-dimensional heterogeneous reservoir models to improve the applicability and predictive capability of the proposed displacement-front characterization method.

5 Conclusions

This study revealed the dynamic evolution characteristics of displacement fronts during chemical flooding in high-water-cut oilfields through two-dimensional visual physical simulation experiments and further quantitatively characterized and mechanistically interpreted their migration laws using reservoir numerical simulation. The main conclusions are as follows:

(1) During chemical flooding, oil-bank migration follows the dynamic evolution law of “formation–accumulation–mobilization–residual”. According to the variation characteristics of water cut, the chemical-flooding process can be divided into three stages: the initial response stage, the peak response stage, and the late response stage. Significant differences exist in oil-bank morphology and migration law among these stages.

(2) The spatiotemporal distributions of the three displacement fronts satisfy the relative positional relationship in which the pressure front leads, the chemical-agent front is in the middle, and the oil-bank front lags behind, reflecting the seepage-flow essence of “pressure propagation before mass transport”. The oil bank is located ahead of the chemical-agent front and consists of an oil–agent mixed zone and a pure oil-bank zone, which together form the core region responsible for production increase during chemical flooding.

(3) Analysis of the main controlling factors shows that heterogeneous flooding forms an oil bank with greater thickness, higher oil saturation, and more uniform accumulation in heterogeneous reservoirs, outperforming binary flooding and polymer flooding. Chemical concentration is the key parameter

controlling oil-bank accumulation intensity; increasing concentration can enlarge the oil-bank size, although diminishing marginal benefits exist. The injected slug size exhibits a threshold effect of approximately 0.4 PV, above which the improvement effect gradually weakens.

(4) Based on the evolution law of displacement fronts and the analysis of the main controlling factors, it is recommended to focus on optimizing the uniform establishment of the pressure field in the initial response stage, strengthening the monitoring and regulation of the chemical-agent-front morphology during the peak response stage, and optimizing the production system in the late response stage to improve oil-bank mobilization efficiency. Through stage-based dynamic control, the peak response period of chemical flooding can be prolonged and the recovery factor can be maximized.

Acknowledgement: We are grateful to Sinopec Shengli Oilfield Company for providing the technical support and research conditions used in this study. We also thank our colleagues and collaborators for their valuable discussions and assistance throughout this work.

Funding Statement: This research was funded by the National Science and Technology Major Project, "New Methods and New Technologies for Significantly Enhancing Oil Recovery in Medium- and High-Permeability Oilfields" (Grant No. 2025ZD1406100), and the Postdoctoral Project of Sinopec Shengli Oilfield Company (Grant No. YKB2502).

Author Contributions: Dejun Wu: Conceptualization, Methodology, Data curation, Software, Investigation, Formal analysis, Visualization, Validation, Writing—original draft, Writing—review & editing. Chunlei Yu: Supervision, Project administration, Funding acquisition, Writing—review & editing. Xuan Lu: Software, Data curation, Visualization, Writing—review & editing. Deshuo Tao: Validation, Investigation, Project administration, Writing—review & editing. Xiaoning Li: Resources, Validation, Writing—review & editing. Hao Song: Investigation, Writing—review & editing. All authors reviewed and approved the final version of the manuscript.

Availability of Data and Materials: Due to the commercial confidentiality and proprietary nature of the reservoir data used in this study, the supporting data cannot be shared publicly. Data may be available from the corresponding author upon reasonable request and with permission from Sinopec Shengli Oilfield Company.

Ethics Approval: Not applicable. This study did not involve human participants, human data, human tissue, or animals, and therefore ethical approval and informed consent were not required.

Conflicts of Interest: The authors declare no conflicts of interest.

References

1. Liu C, Zhou W, Jiang J, Shang F, He H, Wang S. Remaining oil distribution and development strategy for offshore unconsolidated sandstone reservoir at ultrahigh water-cut stage. Geofluids. 2022;2022:6856298. [CrossRef].
2. Yu H, Wang Y, Zhang L, Zhang Q, Guo Z, Wang B, et al. Remaining oil distribution characteristics in an oil reservoir with ultra-high water-cut. Energy Geosci. 2024;5(1):100116. [CrossRef].
3. Sun H, Yang Y, Wang H, Wang J, Wu G, Cui Y, et al. Distribution characteristics of remaining oil in extra-high water cut reservoirs and new technologies for enhancing oil recovery. J China Univ Pet. 2023;47(5):90–102. (In Chinese).
4. Zhang C, Jiang S, Kong X, Jiang Z, Song Y, Dong Y, et al. What controls oil saturation in fractures? J Earth Sci. 2025;36(3):1315–9. [CrossRef].
5. Gong W, Liu Y, Xi C, Yang G, Ju Y, Wang M. Dynamic characterization of residual oil during long-term waterflooding experiments in heterogeneous porous structures. Fuel. 2024;356:129567. [CrossRef].
6. Xu Z, Sun M, Tao L, Bai J, Shi W, Zhang N, et al. Mechanisms of mobility control and enhanced oil recovery of weak gels in heterogeneous reservoirs. Gels. 2025;11(11):854. [CrossRef].
7. An Y, Yao X, Zhong J, Pang S, Xie H. Enhancement of oil recovery by surfactant-polymer synergy flooding: a review. Polym Polym Compos. 2022;30:09673911221145834. [CrossRef].

8. Pi Y, Su Z, Cao R, Li B, Liu J, Fan X, et al. Experimental study on enhanced oil recovery of PPG/ASP heterogeneous system after polymer flooding. Gels. 2023;9(5):427. [CrossRef].
9. Liu Y, Ge L, Ma K, Chen X, Zhu Z, Hou J. Study on surfactant–polymer flooding after polymer flooding in high-permeability heterogeneous offshore oilfields: a case study of Bohai S oilfield. Polymers. 2024;16(14):2004. [CrossRef].
10. Zhang X, Zhang Y, Liu H, Li S, Liu L. Dynamic sweep experiments on a heterogeneous phase composite system based on branched-preformed particle gel in high water-cut reservoirs after polymer flooding. Gels. 2023;9(5):364. [CrossRef].
11. Liu Z, Zhao G, Brewer M, Lv Q, Sudhölter EJR. Comprehensive review on surfactant adsorption on mineral surfaces in chemical enhanced oil recovery. Adv Colloid Interface Sci. 2021;294:102467. [CrossRef].
12. Lv J, Liao G, Liu W, Wang X, Jing Y, Liu H, et al. Effect of reservoir heterogeneity on polymer-surfactant binary chemical flooding efficiency in conglomerate reservoirs. Polymers. 2024;16(23):3405. [CrossRef].
13. Nagy R, Hartyányi M, Bejczi R, Bartha L, Puskás S. Recent aspects of chemical enhanced oil recovery. Chem Pap. 2025;79(5):2695–716. [CrossRef].
14. Yang X, Shen W, Li X, Xie K, Chen J, Li N, et al. Numerical simulation study on parameter optimization of crosslinked polymer flooding for enhanced oil recovery in heavy oil reservoirs. J Petrol Explor Prod Technol. 2025;15:189. [CrossRef].
15. Zhang Y, Gai C, Song B, Jiang J, Wang Z. The influence of permeability and heterogeneity on chemical flooding efficiency and remaining oil distribution-based on NMR displacement imaging. Sci Rep. 2023;13(1):14316. [CrossRef].
16. An ZB, Zhou K, Wu DJ, Hou J. Production characteristics and displacement mechanisms of infilling polymer-surfactant-preformed particle gel flooding in post-polymer flooding reservoirs: a review of practice in Ng3 block of Gudao Oilfield. Petrol Sci. 2023;20(4):2354–71. [CrossRef].
17. Zhang X, Yu J, Liu L, Liu X, Lu X, Feng Q. Experimental investigation of synergistic enhanced oil recovery by infill well pattern and chemical flooding after polymer flooding. Gels. 2025;11(8):660. [CrossRef].
18. Tao L, Wu M, Zhang N, Shi W, Bai J, Xu Z, et al. Investigation on EOR by composite surfactant-polymer (SP) flooding and streamline adjustment through well pattern encryption: a case study of Shengli's strong heterogeneous reservoir. Fuel. 2025;385:134189. [CrossRef].
19. AlZahrani HM, Bijeljic B, Chai R, Blunt MJ. Pore-scale analysis and visualization of tertiary cationic surfactant flooding in a complex carbonate. ACS Omega. 2025;10(43):51383–95. [CrossRef].
20. Hu B, Chai G, Liu X, Wen X, Gu Z, Xie L, et al. Insights into the microscopic oil–water flow characteristics and displacement mechanisms during waterflooding in sandstone reservoir rock based on micro-CT technology: a pore-scale numerical simulation study. Materials. 2023;16(9):3555. [CrossRef].
21. Fernandes BRB, Sepehrnoori K, Delshad M, Marcondes F. New fully implicit formulations for the multicomponent surfactant-polymer flooding reservoir simulation. Appl Math Model. 2022;105:751–99. [CrossRef].
22. Pi Y, Fan X, Liu L, Zhao M, Jiang L, Cheng G. Experimental study on enhanced oil recovery of adaptive system after polymer flooding. Polymers. 2023;15(17):3523. [CrossRef].